Assessing Implicit and Explicit Polarizable Solvation Models for Nuclear–Electronic Orbital Systems: Quantum Proton Polarization and Solvation Energetics

Eleftherios Lambros,[†,§] Benjamin Link,[†,§] Mathew Chow,[‡,§] Filippo Lipparini,[¶] Sharon Hammes-Schiffer,[*,‡] and Xiaosong Li[*,†]

[†]*Department of Chemistry, University of Washington, Seattle, WA, 98195*

[‡]*Department of Chemistry, Yale University, New Haven, CT 06520, USA*

[¶]*Dipartimento di Chimica e Chimica Industriale, Università di Pisa, Via G. Moruzzi 13, 56124 Pisa, Italy*

[§]*These authors contributed equally to this work*

E-mail: sharon.hammes-schiffer@yale.edu; xsli@uw.edu

Abstract

Accurate simulations of many chemical processes require the inclusion of both nuclear quantum effects and a solvent environment. The nuclear-electronic orbital (NEO) approach, which treats electrons and select nuclei quantum mechanically on the same level, combined with a polarizable continuum model (PCM) for the solvent environment, addresses this challenge in a computationally practical manner. In this work, the NEO-PCM approach is extended beyond the IEF-PCM (integral equation formalism PCM) and C-PCM (conductor PCM) approaches to the SS(V)PE (surface and

simulation of volume polarization for electrostatics) and ddCOSMO (domain decomposed conductor-like screening model) approaches. IEF-PCM, SS(V)PE, C-PCM, and ddCOSMO all exhibit similar solvation energetics as well as comparable nuclear polarization within the NEO framework. The calculations show that the nuclear density does not leak out of the molecular cavity because it is much more localized than the electronic density. Finally, the polarization of quantized protons is analyzed in both continuum solvent and explicit solvent environments described by the polarizable MB-pol model, illustrating the impact of specific hydrogen-bonding interactions captured only by explicit solvation. These calculations highlight the relationship between solvation formalism, nuclear polarization, and energetics.

1 Introduction

Continuum solvation models that represent the solvent using a uniform dielectric can be used to describe solvation in systems where an explicit description of the solvent is unaffordable or impractical. These schemes have seen wide success for conventional electronic structure calculations, where their simple parameterization and ease of use allow for a simple yet effective technique to capture solvation effects on a solute molecule.[1,2] In continuum solvation models, the solute molecule is embedded in a cavity, and the solvent is described using a uniform continuum whose polarization response is governed by a dielectric constant.[1,2] The solvent polarization is represented by an effective charge density on the cavity surface, which is calculated using Gauss's law under the effect of the solute electrostatic potential. Among these models, the dielectric and conductor based schemes have emerged as the two major paradigms in the field. The former are derived based on the normal boundary conditions between two media of different dielectric, while the latter use the vanishing surface potential on a conductor surface. Conductor-based models are in principle valid for highly polarizable solvents with large dielectric constants, but they have been shown to provide an accurate description in the lower dielectric regime as well. For example, the conductor-like screen-

ing model (COSMO)[3] and conductor-like polarizable continuum model (C-PCM)[4,5] have been shown to work well for neutral and ionic species, respectively, with small dielectric constants.[6] Each of these models calculates the solvation free energy in terms of the electrostatic interaction between the surface charge density representing the solvent polarization and the electronic and nuclear components of the solute. Such models differ from hybrid quantum mechanical/molecular mechanical (QM/MM) schemes, which offer an explicitly atomistic description of the solvent, usually represented by a force field model.[7]

In a separate vein, the nuclear–electron orbital (NEO) method can be used to incorporate nuclear quantum effects in a molecular system.[8] Unlike other schemes such as path integral techniques,[9,10] the NEO method represents the electronic and quantum nuclear components on the same quantum mechanical footing, naturally avoiding the Born-Oppenheimer separation between electrons and quantum nuclei. This is useful for processes in the non-adiabatic regime, such as proton-coupled electron transfer or hydrogen tunneling, which need a rigorous description of nuclear quantum effects to account for zero point energies, proton delocalization, and other purely quantum mechanical effects on the nuclei. For these processes, the NEO approach has been adapted to real-time (RT) propagation of the electronic and quantum nuclear subsystems in RT-NEO,[11] and within a semiclassical propagation regime using NEO-Ehrenfest dynamics.[12–15] The NEO approach has been derived for Hartree-Fock and density functional theories,[8,16–18] as well as for more advanced wavefunction approaches including second-order Møller-Plesset perturbation theory (MP2) and coupled cluster theory with single and double excitations (CCSD).[19–21]

Although continuum models have been well-characterized for conventional electronic structure methods and force fields, their properties for systems beyond the Born-Oppenheimer regime remain largely unexplored. One such property is the relationship between quantum nuclei and cavity shape. The cavity is generally constructed from a union of atomic spheres centered on each classical nucleus.[22] The cavity size can then be empirically tuned by scaling the radius about each nuclear position, which is usually chosen from a set of atomic or van

der Waals (vdW) radii.[23] In systems with quantum mechanical nuclei, it is not yet clear how classically generated cavities affect the solvation properties of the system. Ambiguities also arise in the generation of molecular cavities for systems where quantum protons move, such as in geometry optimizations and dynamics simulations, relating to proton delocalization about the nuclear basis function centers. It is also well-known that in standard electronic structure calculations, these schemes can be affected by the outlying charge problem, where a portion of the electronic density extends beyond the cavity surface and into the continuum, resulting in energetic artifacts.[24–26]

Another point of interest is how different solvent models affect the solvation properties of quantum nuclei. Within the dielectric and conductor paradigms, there exist several variations of these formalisms. Dielectric models include dielectric PCM (D-PCM),[27] variational PCM (V-PCM),[28] surface and simulation of volume polarization for electrostatics (SS(V)PE),[29,30] and integral equation formalism PCM (IEF-PCM).[31–33] Conductor models include the conductor-like screening model (COSMO),[3] conductor PCM (C-PCM),[4,5]and generalized G-COSMO.[34–38] Each of these models uses a different response matrix, which was formulated to satisfy various criteria. D-PCM, for example, is formulated directly from the dielectric boundary conditions and uses the electric field normal to the cavity surface to derive a corresponding set of apparent surface charges. The more modern IEF-PCM and SS(V)PE models are based on an alternate derivation using the electrostatic potential on the cavity due to the solute, and they use an asymmetric response matrix to generate the surface charges.[29–33] Conductor models such as COSMO, G-COSMO, and C-PCM use a simpler, symmetric response matrix formulated from the vanishing potential property on a conductive surface.[3,5,35] How each of these models affects the solvation properties of quantum nuclei is an open question.

Efforts to incorporate solvation effects into the NEO approach[15,39,40] and other related multicomponent methods[41,42] have coupled the quantum mechanical system to IEF-PCM.[31–33] A previous study demonstrated that the nuclear density can be directly polarized by a sol-

vent environment, and quantum protons will differentially polarize depending on their local environment.[39] Herein, we provide an extensive analysis of solvated NEO systems in continuum models, including the IEF-PCM, SS(V)PE, C-PCM, and ddCOSMO approaches. We characterize the energetic properties of NEO molecular systems combined with continuum solvation models and compare the proton polarization between these methods. Furthermore, the outlying charge problem is investigated within the NEO framework, examining the interplay between cavity shape and size, solvation free energy, and outlying charge. Finally, we build off of previous work developing a NEO-QM/MM approach[40] and characterize the properties of NEO molecular systems in an explicit solvent described by the MB-pol[43–45] model compared to a polarizable continuum representation.

2 Theory and Computational Details

2.1 Nuclear-Electron Orbital Method

The NEO method partitions a system into electrons, classical nuclei, and quantum nuclei, assumed here to be protons for convenience. For single-determinant methods such as HF or DFT, the wavefunction ansatz is expressed as a product of the electronic and quantum nuclear components:

$$\Psi_{\mathrm{NEO}}(\mathbf{x}^e, \mathbf{x}^p; \mathbf{r}^c) = \Phi_e(\mathbf{x}^e; \mathbf{r}^c)\Phi_p(\mathbf{x}^p; \mathbf{r}^c) \tag{1}$$

where Φ_e is the electronic determinant and Φ_p is the determinant for the quantum protons. Here $\mathbf{r}^c$, $\mathbf{x}^e$, and $\mathbf{x}^p$ correspond to the classical nuclear positions and collective spatial-spin coordinates of the electrons and quantum protons, respectively. The energy in the NEO-DFT[16,18,46] approach can be expressed as:

$$E = E_{\mathrm{ext}} + E_{\mathrm{ref}} + E_{\mathrm{exc}} + E_{\mathrm{pxc}} + E_{\mathrm{epc}} \tag{2}$$

where E_{ext} captures the interaction of the electronic and protonic densities with the external potential of the classical nuclei, and E_{ref} includes the non-interacting kinetic energies, as well as the Coulomb interactions among the electrons and quantum protons. E_{exc}, E_{pxc}, and E_{epc} correspond to the electron-electron exchange-correlation, the proton-proton exchange-correlation, and the electron-proton correlation energies. E_{pxc} is negligible because of the spatial localization of the protons and is thus equated to the diagonal terms of exact exchange in order to formally remove Coulombic self-interaction, although in practice all proton-proton exchange terms may be included. Since electrons and protons are non-identical particles, there is no exchange between them.

In NEO-DFT calculations, the electronic and nuclear Kohn-Sham equations are iteratively solved until self-consistency is achieved. This produces a ground state nuclear-electronic wavefunction from which the total energy, as well as the electronic and protonic densities, is calculated.

2.2 Continuum Solvation models

The continuum solvation model formalism describes an equilibrium solvent environment using a single parameter, the static dielectric constant ε_s, which describes the ability of the solvent to screen charge relative to the vacuum permittivity ε_0.[1,2] Non-equilibrium continuum solvation uses an additional optical dielectric constant ε_{opt}, which governs the fast polarization response. The advantage of continuum solvation comes from the highly coarse-grained representation of the environment. This eliminates the need to sample over the many solvent degrees of freedom since all the homogeneous solvent information is implicitly encoded in the dielectric constant. As such, continuum solvation models are attractive for electronic structure calculations that steeply scale with system size. It should be noted that this scheme cannot capture explicit solvent effects such as hydrogen bonding and other atomically-resolved interactions.

Dielectric continuum theory is a purely electrostatic theory and does not inherently cap-

ture the finite size of a molecule. Because of this, it is necessary to generate a molecular cavity in order to define an interface between the solute and the continuum solvent. These cavities are generally defined in terms of atomic vdW radii and, in some cases, can be constructed from the molecular isodensity surface if the system is represented with an electronic structure approach.[2] Once a cavity has been defined, the continuum solvation model equations are derived from the dielectric or conductor boundary conditions at the cavity surface. In the reaction field formalism, the electrostatic solvation free energy is expressed as the interaction of the surface charge density σ with the solute's electrostatic potential v^{solute}

$$G_s = \frac{1}{2} f_\varepsilon \int_{\partial\Omega} v^{\text{solute}}(\mathbf{s})\sigma(\mathbf{s})d\mathbf{s} \tag{3}$$

where $\partial\Omega$ denotes the cavity surface.

In practice, the surface charge density is discretized to a set of apparent surface charges, $\mathbf{q}$, and the problem is recast as a set of linear equations. The surface charges are calculated from the solute electrostatic potential on the cavity surface, $\mathbf{v}$, using the following equations:

$$\mathbf{Kq} = \mathbf{Rv} \tag{4}$$

Here, $\mathbf{K}$ and $\mathbf{R}$ govern the electrostatic interactions between surface charges, as well as any necessary boundary conditions. Table 1 summarizes the models examined in this paper. $\mathbf{S}$

Table 1. Summary of the PCM Methods

Method	$\mathbf{K}$	$\mathbf{R}$	scalar f_ε	References
IEF-PCM	$\mathbf{S} - \frac{f_\varepsilon}{2\pi}\mathbf{DAS}$	$-f_\varepsilon(I - \frac{1}{2\pi}\mathbf{DA})$	$(\varepsilon-1)/(\varepsilon+1)$	31–33
SS(V)PE	$\mathbf{S} - \frac{f_\varepsilon}{4\pi}(\mathbf{DAS} + \mathbf{SAD}^\dagger)$	$-f_\varepsilon(I - \frac{1}{2\pi}\mathbf{DA})$	$(\varepsilon-1)/(\varepsilon+1)$	29,30
C-PCM	$\mathbf{S}$	$-f_\varepsilon\mathbf{I}$	$(\varepsilon-1)/(\varepsilon)$	4,5
COSMO	$\mathbf{S}$	$-f_\varepsilon\mathbf{I}$	$(\varepsilon-1)/(\varepsilon+1/2)$	3

describes the Coulomb interaction between surface charges, $\mathbf{D}$ generates the potential of a dipolar surface charge distribution, and $\mathbf{A}$ is the surface area of each cavity tessera. The $\mathbf{D}$ matrix arises from the dielectric boundary conditions used in the IEF-PCM and SS(V)PE

models. f_e is the permitivitty dependent scaling factor, which is an empirically modified form of the D-PCM prefactor.[27] The functional forms of the **K** and **R** matrices depend on the specific model, and detailed derivations of these are given in the references provided in Table 1. The IEF-PCM and SS(V)PE methods belong to the dielectric type scheme and differ only in their representation of the **K** matrix. The C-PCM and COSMO methods are conductor-like models that differ only in the representation of the scalar f_ε for the dielectric screening. Historically COSMO may refer to the original dual cavity implementation of the model, which accounts for the outlying charge,[3] although in this work all models use the same single cavity. It has been shown that the C-PCM and COSMO formulations already include an implicit outlying charge correction even without the dual cavity.[2,25]

We also examine these models within the Schwarz domain decomposition, which allows the **K** matrix to be block-sparse but does not change the fundamental screening electrostatics. Domain decomposition allows for up to linear scaling algorithms to be used to invert the response matrix. ddCOSMO is the domain decomposed version of C-PCM[47–49] because the reference implementation of ddCOSMO used the C-PCM scalar $f_\varepsilon = (\varepsilon - 1)/(\varepsilon)$ rather than the COSMO scalar $f_\varepsilon = (\varepsilon - 1)/(\varepsilon + 1/2)$.[49] ddPCM is the domain decomposed version of IEF-PCM.[50,51]

The extension of the continuum solvation models to NEO calculations is straightforward, mainly involving the calculation of the quantum proton potential on the cavity surface and the inclusion of the solvation polarization term in the protonic Kohn-Sham equations.[15,39,40] The ddCOSMO derivation is slightly more involved, so a more detailed extension to NEO calculations is described in the SI. The cavity for NEO calculations is constructed in the same manner as for the conventional electronic structure counterpart, with the quantum proton position represented by its basis function center position. As the geometry of the molecule changes, or the proton basis function center moves beyond the cavity due to a process such as proton transfer, the cavity must be constructed again, analogous to the conventional electronic continuum solvation methods.

2.3 Polarizable QM/MM with MB-pol

In this study, we also couple NEO to the MB-pol polarizable force field in a polarizable embedding QM/MM scheme, denoted by NEO-QM/MB-pol. MB-pol contains inducible point dipoles on each atomic site, thereby allowing the solvent to polarize in response to changes in the solute's electronic and nuclear densities. Furthermore, MB-pol is advantageous because it is trained on the CCSD(T) potential energy surface and provides the most accurate representation of water across all phases.[43–45,52] A more general discussion of inducible dipole force fields can be found in the relevant literature.[53] Because MB-pol is variational with respect to the dipole polarization, the fundamental QM/MM interaction can be written as a variational functional of the density matrix $\mathbf{P}$, which includes both the electronic and quantum nuclear contributions, and the inducible point dipoles $\boldsymbol{\mu}$:[54]

$$\mathcal{E}(\mathbf{P}, \boldsymbol{\mu}) = \mathcal{E}^{\mathrm{QM}}(\mathbf{P}) + \mathcal{E}^{\mathrm{MM}}(\boldsymbol{\mu}) + \mathcal{E}^{\mathrm{Int}}(\mathbf{P}, \boldsymbol{\mu}) \tag{5}$$

where $\mathcal{E}^{\mathrm{Int}}$ describes the interaction between the QM and MM regions, written as $\mathcal{E}^{\mathrm{Int}} = \mathcal{E}^{\mathrm{Pol}} + \mathcal{E}^{\mathrm{Perm}} + \mathcal{E}^{\text{Non-elec}}$. These terms govern the polarization, permanent electrostatic, and non-electrostatic interactions, respectively. Within $\mathcal{E}^{\mathrm{Int}}$, the polarization plays a particularly important role, as it allows dynamic communication between the two regions. Formally, the polarization is expressed as the interaction of the MM dipoles with the QM electric field:

$$\mathcal{E}^{\mathrm{Pol}}(\mathbf{P}, \boldsymbol{\mu}) = \frac{1}{2}\boldsymbol{\mu}^{\dagger}\mathbf{T}\boldsymbol{\mu} - \boldsymbol{\mu}^{\dagger}(\mathbf{E}^{\mathrm{MM}} + \mathbf{E}^{\mathrm{QM}}(\mathbf{P})), \tag{6}$$

Here, $\mathbf{E}^{\mathrm{QM}}$ is the electric field due to the electronic, classical nuclear, and quantum nuclear components of the QM subsystem, $\mathbf{E}^{\mathrm{MM}}$ is the electric field arising from the permanent partial charges in the MM region, and $\mathbf{T}$ describes the Thole-damped dipole interaction tensor.

In this scheme, the induced dipoles are obtained by solving the dipole equation at each

SCF step:

$$\boldsymbol{\mu} = \mathbf{A}^{-1}(\mathbf{E}^{\mathrm{MM}} + \mathbf{E}^{\mathrm{QM}}(\mathbf{P})) \tag{7}$$

where $\mathbf{A}$ is the matrix that governs the molecular response to an external field:

$$\mathbf{A} = \begin{bmatrix} -\hat{a}_1^{-1} & \mathbf{T}_{12} & \dots & \mathbf{T}_{1N_\mu} \\ \mathbf{T}_{21} & -\hat{a}_2^{-1} & \dots & \mathbf{T}_{2N_\mu} \\ \vdots & \vdots & \ddots & \vdots \\ \mathbf{T}_{N_\mu 1} & \mathbf{T}_{N_\mu 2} & \dots & -\hat{a}_{N_\mu}^{-1} \end{bmatrix} \tag{8}$$

Here, $\hat{a}$ is the atomic polarizability tensor for each respective atom, and N_μ is the total number of atoms.

2.4 Computational Details

All calculations in this study were performed using a development version of Chronus Quantum[55] using the PBE0[56] and epc17-2[18] functionals for the electronic exchange-correlation and electron-proton correlation, respectively. Calculations were performed on the geometry of the water dimer optimized in vacuum using CCSD(T)/CBS from the A24 dataset.[57] IEF-PCM, C-PCM, and SS(V)PE were correspondingly validated against the implementation in Q-Chem.[58] ddCOSMO (non-NEO) was validated against the corresponding implementation in PySCF.[59,60] Calculations with ddCOSMO used $l_{max} = 10$ for the truncation of the spherical harmonic basis and used a regularization parameter $\eta = 0.0$ (no switching) to ensure the ddCOSMO cavity was consistent with the IEF-PCM, SS(V)PE, and C-PCM cavities.[49,50] The cc-pVTZ[61] basis set was used for the electronic subsystem, and the PB4-D[62] protonic basis set was used for the quantum protons. A (99,590) grid was used for the DFT numerical integration. The molecular cavities were constructed using the corresponding UFF radii scaled by 1.1 and using 590 surface grid points per atom, corresponding to a 41st order Lebedev grid. The MBX library[63] was coupled with ChronusQ to use the MB-pol model in

a polarizable embedding QM/MM scheme.

3 Results and Discussion

3.1 Comparison of Solvent Models for Solvation Free Energy Calculations

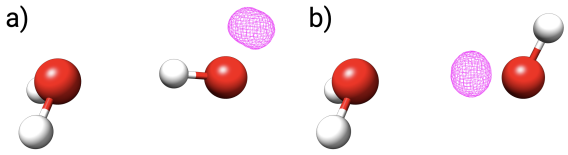

Figure 1. Geometry of the water dimer with a) the external proton treated quantum mechanically and b) the internal proton treated quantum mechanically.

Here, we examine the differences in solvation free energy as a function of dielectric constant for a water dimer (Figure 1) using the IEF-PCM, SS(V)PE, C-PCM, and ddCOSMO (the domain decomposition variant of C-PCM) methods. Figure 2 plots the solvation free energy obtained with conventional electronic and NEO calculations for these solvation models. Only the external proton (Figure 1a) was treated quantum mechanically for these NEO calculations in order to isolate the effect of one quantum proton. An analysis of cases with multiple quantum protons is provided in the following subsection. In the conventional case (*i.e.*, classical proton), IEF-PCM, SS(V)PE, C-PCM, and ddCOSMO converge to a solvation free energy of ∼-7.8 – -8.0 kcal/mol as $\varepsilon \rightarrow 100$. For the NEO calculations, the solvation free energy converges to a value of ∼-8.0 – -8.2 kcal/mol as $\varepsilon \rightarrow 100$ for all four solvation models, suggesting an increase of ∼0.3 kcal/mol in solvation free energy induced by the quantum nature of the proton. These results suggest that for polar solvents with dielectric constants greater than ∼20, the electrostatic solvation free energy is qualitatively similar for the IEF-PCM, SS(V)PE, C-PCM, and ddCOSMO models.

Next we seek to understand how increasing the number of quantum protons in a system will modulate the solvation free energy. Figure 3 plots the distribution of solvation free

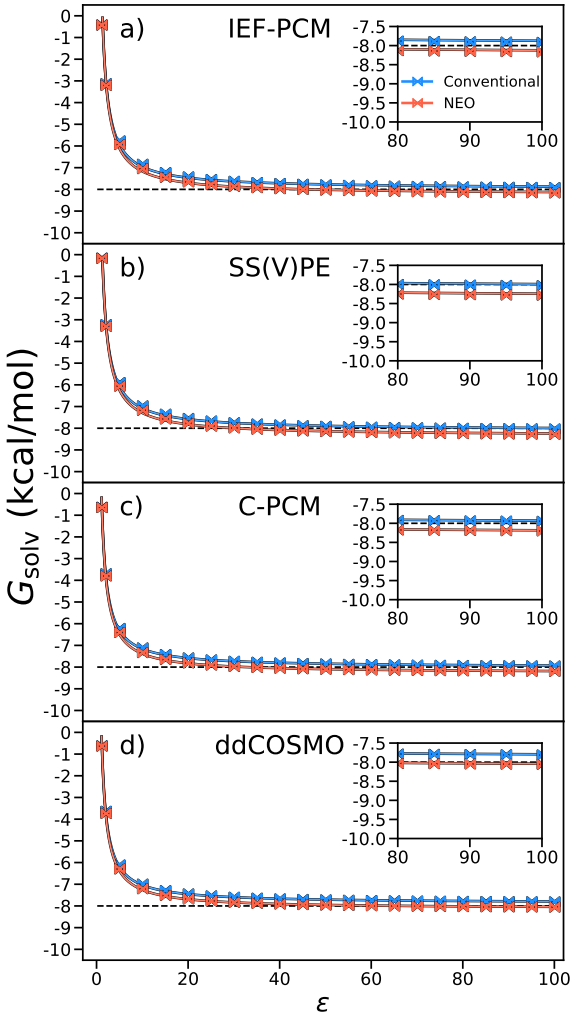

Figure 2. Electrostatic solvation free energy as a function of dielectric constant for a water dimer examined with the **a)** IEF-PCM, **b)** SS(V)PE, **c)** C-PCM, and **d)** ddCOSMO approaches. The NEO and conventional cases are shown in red and blue, respectively.

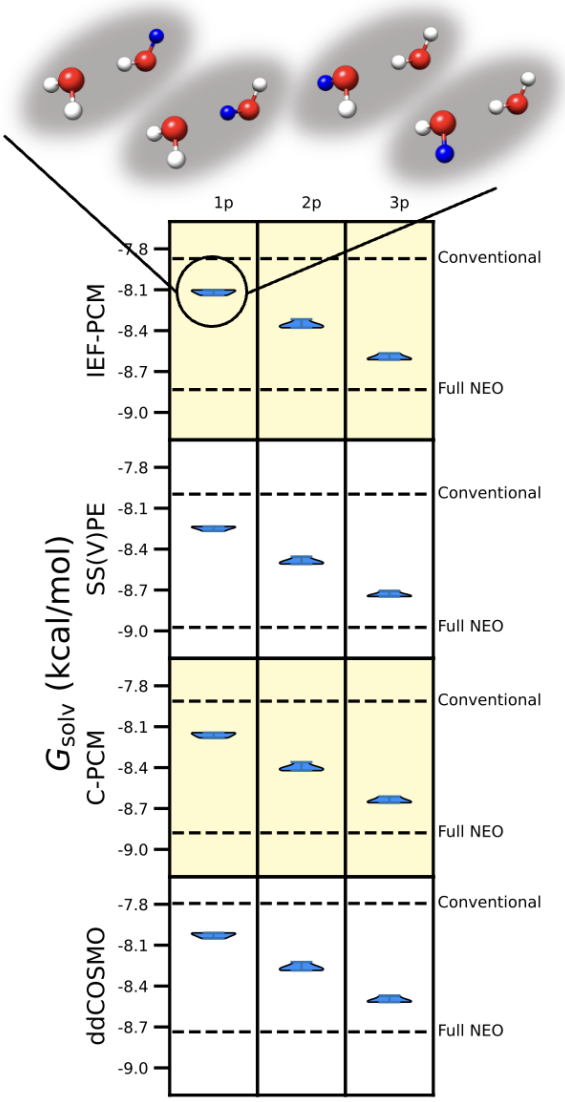

Figure 3. Electrostatic solvation free energy as a function of number of quantum protons for a water dimer examined using the IEF-PCM, SS(V)PE, C-PCM, and ddCOSMO methods with $\varepsilon = 78.3553$. The left, middle, and right panels describe a water dimer with 1, 2, and 3 quantum protons, respectively. The schematic at the top of the figure shows all possible ways to treat a water dimer with 1 quantum proton colored in blue. The conventional electronic and full NEO results, corresponding to 0 and 4 quantum protons, respectively, are shown with horizontal dashed lines.

energies for a water dimer with one, two, and three quantum protons in a solvent with $\varepsilon = 78.3553$. The cases with zero and four quantum protons represent the conventional electronic and full NEO calculations, respectively, and are depicted as horizontal dashed lines. There are four, six, and four possible ways to choose one, two, and three quantum protons, respectively, in the water dimer system. This results in a distribution of free energies for the cases with one, two, and three quantum protons, as demonstrated in Figure 3.

Starting from the conventional electronic case and successively adding one proton to the quantum nuclear subsystem, it is observed that for IEF-PCM, SS(V)PE, C-PCM, and dd-COSMO, the solvation free energy decreases by about 0.3 kcal/mol per additional quantum proton. Despite the narrow free energy distribution seen for each step, dimer configurations containing an internal quantum proton exhibit a slightly greater solvation free energy than the configurations with an external quantum proton. Table S1 in the Supporting Information shows the raw free energy values for each possible way to form a NEO water dimer with a corresponding schematic. The general decrease in solvation free energy observed at each step is consistent with the results in Figure 2, where the solvation free energy for the NEO dimer with the external proton quantized was $\sim$0.3 kcal/mol more negative than the conventional case for $\varepsilon > \sim 20$. This lowering of solvation free energy is a result of the quantum nucleus being able to self-consistently interact with the apparent surface charges on the cavity. Because the proton is treated quantum mechanically, the density can polarize and respond to changes in the solvent, leading to a stronger interaction. However, there is also an interplay between the proton and electron densities, and the changes in solvation free energy are likely the result of concerted protonic and electronic polarization.

In order to extend our analysis to a broader set of molecular species, we performed additional calculations for all species in the A24 dataset, which is composed of small molecular dimers.[57] Figure 4 plots the difference in electrostatic solvation free energy per quantum

proton between a NEO and conventional calculation, defined as:

$$\delta G = (G_s^{\mathrm{NEO}} - G_s^{\mathrm{Conv}})/N_{\mathrm{prot}}. \tag{9}$$

This quantity is correlated against the magnitude of the molecular dipole moment in vacuum and the total number of protons, N_{prot}, for these species. In this analysis, all protons are treated quantum mechanically for the NEO calculations, and the data is plotted for the IEF-PCM method. Additional data for the C-PCM, SS(V)PE, and ddCOSMO methods are included in the SI. Figure 4 shows that the increase in solvation free energy per quantum proton varies over ∼0.5 kcal/mol, indicating that the ∼0.3 kcal/mol increase per quantum proton observed for the water dimer is not a general phenomenon. Moreover, dimers with a larger number of protons typically have smaller changes in solvation free energy.

To gain a deeper physical understanding of these results, the solvation free energy data is correlated against the magnitude of the vaccuum molecular dipole moment in Figure 4a. This data shows that the more polar species, indicated by greater dipole magnitude, typically exhibit a larger increase in solvation free energy per proton with NEO. A greater cavity polarization induced by a larger dipole will correspondingly lead to a stronger proton polarization response. This suggests that polar species are often more sensitive to nuclear quantization in solvation schemes than are non-polar species. This analysis suggests an interplay among molecular polarity, proton and electron polarization, and the solvent response.

3.2 Dependence of Proton Polarization on Implicit Solvation Model

Following the previous analysis, this subsection examines the differences in proton polarization among the various popular polarizable continuum models. The proton polarization for the internal and external protons in the water dimer are plotted in Figure 5, calculated using IEF-PCM, SS(V)PE, C-PCM, and ddCOSMO with $\varepsilon = 78.35$. The proton polarization is defined in this work as the density difference between the solvated and vacuum phase

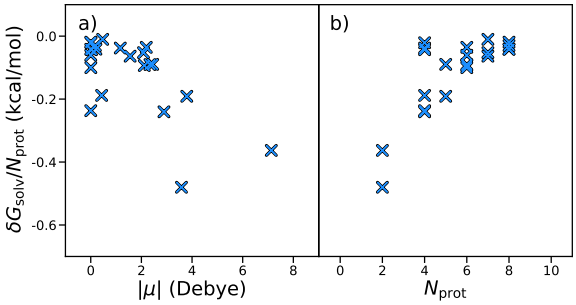

Figure 4. Difference in electrostatic solvation free energy per proton between NEO and conventional calculations for species in the A24 dataset as a function of **a)** magnitude of the vaccuum dipole moment and **b)** total number of protons in the system using the IEF-PCM method with $\varepsilon = 78.35$. Data corresponding to the C-PCM, SS(V)PE, and ddCOSMO methods is provided in the SI.

quantum proton densities:

$$\Delta\rho_{\text{proton}}(\mathbf{r}) = \rho_{\text{solv}}(\mathbf{r}) - \rho_{\text{vac}}(\mathbf{r}). \tag{10}$$

The proton polarization can be quantitatively described by the difference of the O-H bond length in solution and in vacuum. The O-H bond length for a quantum proton is calculated as

$$r_{\text{OH}} = |\mathbf{r}_{\text{O}} - \langle\psi_p|\mathbf{r}|\psi_p\rangle| \tag{11}$$

where ψ_p is the variationally optimized[15,64] orbital for the quantum mechanical proton, and $\mathbf{r}_{\text{O}}$ is the classical oxygen position. Although the basis function centers for the quantum protons are fixed to the original classical positions, the PB4-D protonic basis set is sufficiently large to capture proton polarization.

The effects of solvation on the O-H bond length are given in Figure 5. In Figure 5(a-d), the polarization response of the external proton is similar for the IEF-PCM, SS(V)PE, C-PCM, and ddCOSMO models. For the hydrogen-bonded internal proton in Figure 5(e-h), a similar trend is observed, where all models display quantitatively similar proton polarization response. More quantitatively, solvation is observed to increase the external O-H bond length by 0.0045 Bohr for the IEF-PCM, SS(V)PE, C-PCM and ddCOSMO models. The internal

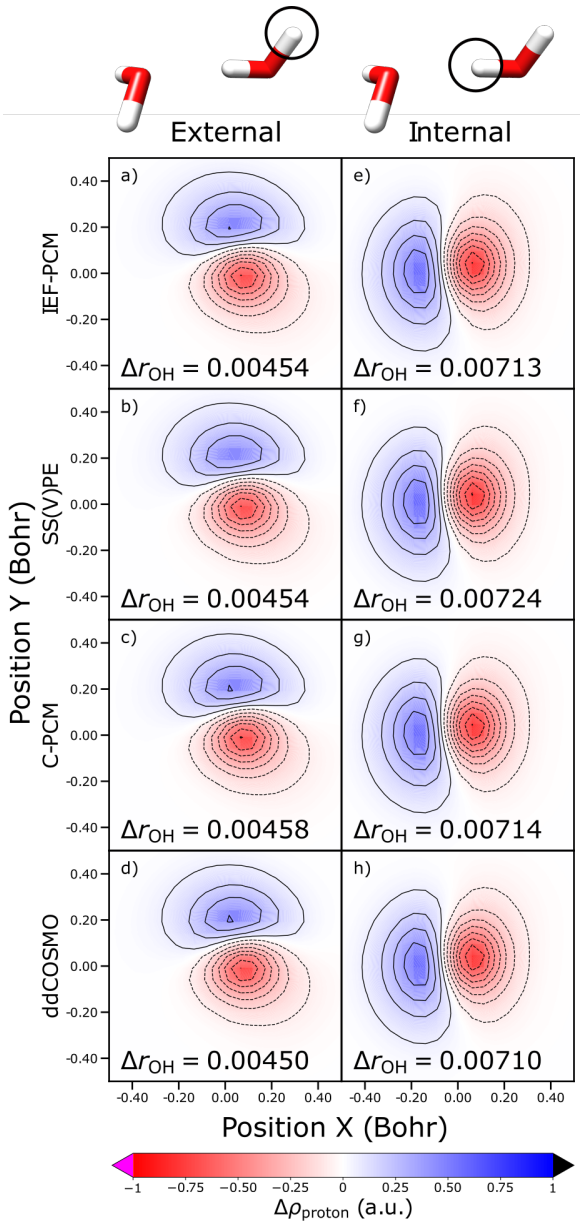

Figure 5. Polarization of the proton density in a water dimer upon solvation. The proton densities were computed with NEO-PCM for a quantum mechanical treatment of **a-d)** the external hydrogen and **e-h)** the internal hydrogen for each continuum solvent model with $\varepsilon = 78.3553$. Changes in O-H bond lengths are shown in Bohr. The density differences are oriented according to the schematic of the dimer on top.

O-H bond length is observed to increase by 0.007 Bohr for all four models. These results are consistent with previous work on the IEF-PCM model.[39]

3.3 Effects of Cavity Size and Shape in NEO systems

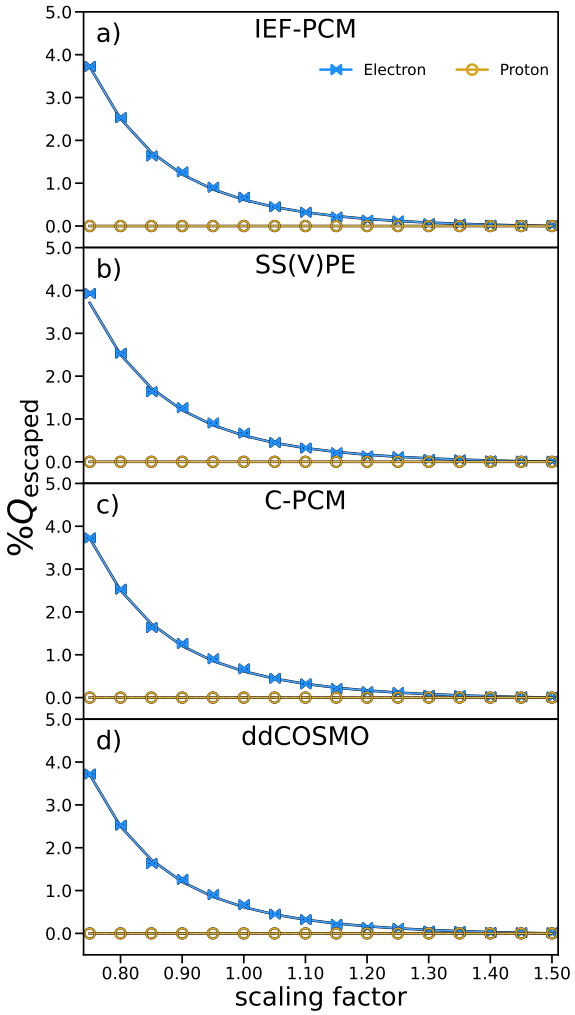

Figure 6. Percentage escaped charge for the electrons and quantum protons as a function of vdW radius scaling factor for a water dimer examined using the **a)** IEF-PCM, **b)** SS(V)PE, **c)** C-PCM, and **d)** ddCOSMO methods with $\varepsilon = 78.3553$ and the UFF radii.

As previously mentioned, since continuum solvation theory does not inherently describe non-electrostatic interactions, the cavity in which the solute is embedded can be generated following various prescriptions. In practice, the cavity for a NEO molecular system is generated from the classical nuclear positions in conjunction with the basis function centers of

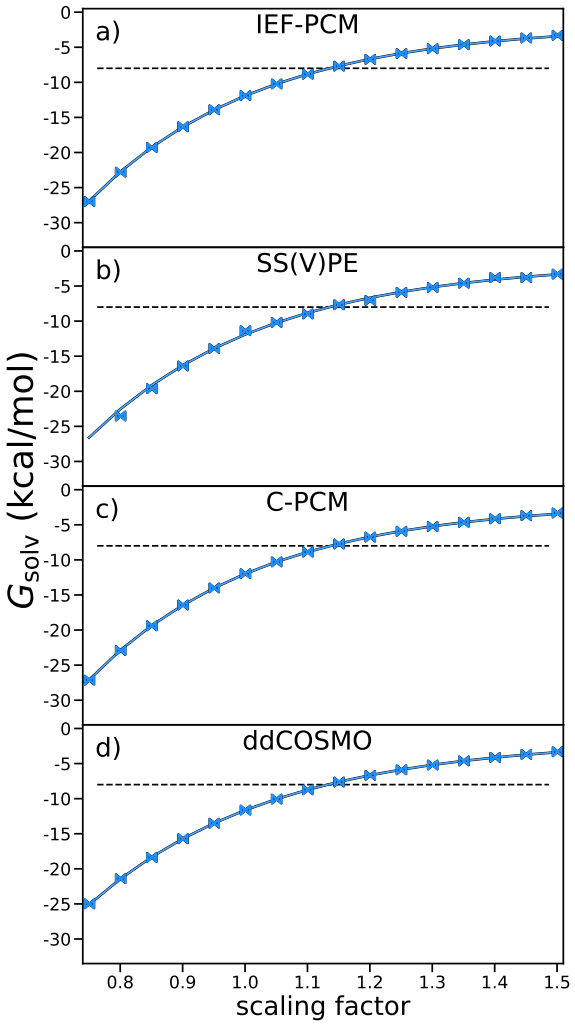

Figure 7. Electrostatic solvation free energy as a function of vdW radius scaling factor for a water dimer examined using the **a)** IEF-PCM, **b)** SS(V)PE, **c)** C-PCM, **d)** and **d)** ddCOSMO methods with $\varepsilon = 78.3553$ and the UFF radii. A dashed line is drawn at -8 kcal/mol as a guide to the eye.

the quantum protons. This subsection investigates the relationship between solvation free energies, outlying charge, and cavity shape for NEO calculations. Figure 6 shows the percentage of escaped charge from the cavity for the electronic and quantum proton densities for each solvation method for vdW radii scaling factors of 0.75 to 1.50. The percentage of escaped charge is calculated by integrating over the volume of the cavity, V, and counting the number of particles contained therein:

$$\%Q_{\text{escaped}} = \frac{Q_{\text{total}} \pm e \int_V \rho(\mathbf{r}) d\mathbf{r}}{Q_{\text{total}}} \times 100 \tag{12}$$

where the sign is dependent on the type of particle. The corresponding solvation free energy is also shown in Figure 7. The UFF radii give $r_{\text{H}}^{\text{vdW}} = 1.443$ Å and $r_{\text{O}}^{\text{vdW}} = 1.75$ Å. At $r = r^{\text{vdW}}$, $\sim$0.7% of the total electronic charge is escaped from the cavity for all models examined. This decreases to $\sim$0.3% at $r = 1.1 \times r^{\text{vdW}}$, which is the default atomic sphere radius used in all previous calculations. The corresponding solvation free energies are ~ -12.0 kcal/mol at $r = r^{\text{vdW}}$, and ~ -8.9 kcal/mol at $r = 1.1 \times r^{\text{vdW}}$. In contrast to the electronic charge, the proton charge is functionally completely contained within the cavity for all examined radii scaling factors and models. This is a result of the relatively localized proton density, as the proton has a significantly greater mass compared to the electron.

These data are consistent with early studies that documented how sensitive the solvation free energy is to molecular cavity size and shape.[31] For the water dimer examined in this study, even a few percent change in the cavity size can result in multi-kcal/mol differences in the solvation free energy. It should be noted that while solvation free energies are rather sensitive to this effect, relative free energies, redox potentials, and pK_{a} values can be quite accurately recovered. Most importantly, this analysis shows that the outlying charge problem is a purely electronic problem for reasonable cavities, as the proton density is highly localized and does not escape the bounds of the cavity for static systems.

3.4 Proton Polarization in Implicit vs Explicit Solvation

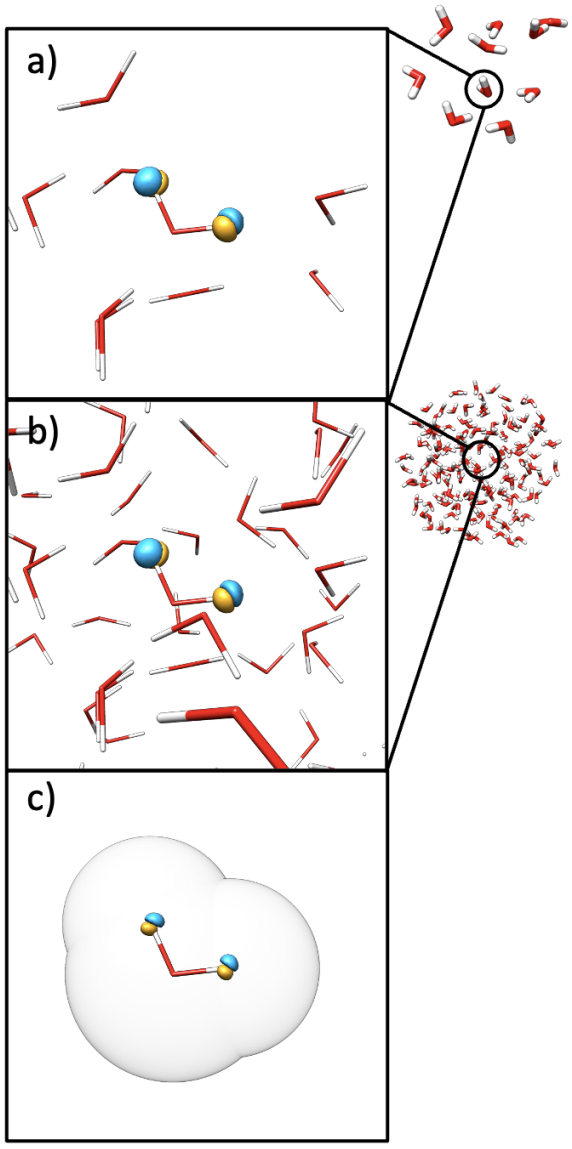

Figure 8. Polarization of the proton density in a water molecule upon solvation by **a)** 10 explicit MB-pol water molecules, **b)** 160 explicit MB-pol water molecules, and **c)** IEF-PCM with $\varepsilon = 78.3553$. An isosurface value of ± 0.1 a.u. was used with blue representing positive values and yellow representing negative values.

Next we examine the differences in proton polarization between a polarizable continuum scheme and an explicit polarizable solvent environment in a prototypical test case of a single water molecule. Figure 8 plots the proton polarization of a water molecule treated with NEO-DFT embedded in a single solvation layer of 10 water molecules, a bulk environment

Table 2. Normalized Molecular Dipole Moment of a NEO Water Molecule in Vacuum and in a Solvent Environment Described Using the MB-pol Model or IEF-PCM with $\varepsilon = 78.35$.

	$\mu_x/\lvert\mu\rvert$	$\mu_y/\lvert\mu\rvert$	$\mu_z/\lvert\mu\rvert$
Vacuum	−0.561	0.355	−0.748
10 MB-pol H_2O	−0.555	0.386	−0.694
160 MB-pol H_2O	−0.573	0.398	−0.716
IEF-PCM	−0.561	0.355	−0.748

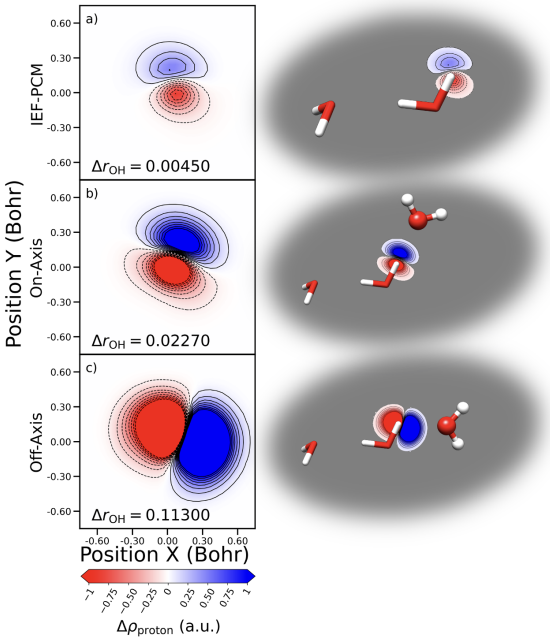

Figure 9. Polarization of the proton density for the proton of a water dimer a) in IEF-PCM with $\varepsilon = 78.3553$, b) interacting with an MB-pol water aligned along the O-H axis, and c) interacting with an MB-pol water aligned off of the O-H axis. A schematic is provided on the right hand side of the figure.

of 160 water molecules, and an IEF-PCM environment. All explicit waters were described using the MB-pol model, and a dielectric constant of $\varepsilon = 78.35$ was used for the IEF-PCM calculation. Because the previous analyses showed that all the examined continuum solvation models displayed quantitatively similar solvation properties, only the IEF-PCM model is considered in this case for brevity. The configurations for Figure 8a and Figure 8b were extracted from a randomly selected frame from an MB-pol centroid molecular dynamics trajectory,[65] including the nearest 10 and nearest 160 water molecules, respectively, to the central water.

The proton densities shown in Figure 8a and Figure 8b are computed relative to the proton density in vacuum for a single NEO-DFT water molecule surrounded by 10 and 160 MB-pol water molecules, respectively, using a polarizable embedding QM/MM scheme. When surrounded by 10 water molecules, the proton polarizes in the direction of the neighboring water molecules that accept the hydrogen bond. The similarity between the proton densities in these two figures indicates that the proton polarization does not qualitatively change when introducing additional solvation layers to the system. Figure 8c shows the proton polarization when the same NEO-DFT water molecule is embedded in an IEF-PCM cavity. In this case, the two protons polarize in a uniform direction toward the cavity surface, in contrast to the explicit solvent cases where the protons polarize non-uniformly in the directions of the hydrogen-bonded explicit water molecules.

For a more quantitative analysis, the normalized molecular dipole moments of the water molecule in vacuum, surrounded by 10 and 160 explicit waters, and in IEF-PCM are given in Table 2. The homogeneous implicit solvation model does not significantly change the molecular dipole moment orientation compared to the vacuum case, consistent with the uniform proton polarization shown in Figure 8c. Furthermore, the 10 and 160 explicit water cases in Table 2 produce a dipole moment direction that is not parallel to the vacuum dipole moment, consistent with the non-uniform proton polarization shown in Figure 8a and Figure 8b. These data suggest that the anisotropy of the local environment can influence

the polarization of the proton. Polarizable continuum models that represent the solvent by a uniform dielectric may not be able to capture important proton polarization arising from an atomistic description of the solvent.

To further characterize the magnitude of proton polarization induced by explicit and implicit solvent representations, Figure 9 depicts the proton polarization for a NEO-DFT water dimer in three different environments: IEF-PCM and coordinating with 1 MB-pol water molecule in two different orientations. The proton polarization and bond length changes are defined by Eq. (10) and Eq. (11), respectively, in Section 3.2. In this analysis, only the external proton, as shown in the schematic on the right side of the figure, is treated quantum mechanically to isolate the polarization effects to a single proton.

The IEF-PCM environment increases the O-H bond length by $\sim$0.0045 Bohr, whereas the MB-pol environment increases the bond length by $\sim$0.02 and $\sim$0.1 Bohr in the two different orientations, respectively. This data also demonstrates that the magnitude of the proton polarization is dependent on the hydrogen bond angle. A more detailed analysis of the MB-pol polarization split between the permanent charge and inducible dipole contributions is provided in Figures S1 and S2. Briefly, the MB-pol model tends to more strongly polarize the quantum proton relative to a PBE0 water molecule. It should be noted in this case that density functional approximations tend to over-delocalize the electronic density, which can lead to long-range energetic and polarization artifacts.

4 Conclusions

This study highlights the differences and similarities among the various continuum solvation formalisms applied to NEO systems. Our calculations demonstrate that the IEF-PCM, SS(V)PE, C-PCM, and ddCOSMO models produce quantitatively similar solvation free energies and bond length changes for NEO systems. Importantly, we show that nuclear quantization can impact the solvation free energies, especially for polar species. This provides

fundamental insight into the interplay among nuclear quantization, the solvent environment, and molecular polarity. We also demonstrate that the outlying charge problem is unique to the electron density, and that the quantum proton density is almost completely contained in a conventional cavity for most systems. The sensitivity of the solvation free energy to cavity size and shape demonstrated in previous studies[31] is reinforced, showing that even a small change in cavity size can result in multi-kcal/mol differences in the solvation free energy. Finally, the proton polarization induced by an implicit solvent environment is compared to that induced by an explicit solvent environment. Our calculations show that the MB-pol model can accurately capture proton polarization induced by specific hydrogen-bonding interactions in a NEO QM/MM scheme. These findings will be useful in guiding future chemical applications of the NEO approach combined with continuum solvation models.

Supporting Information

The supporting information includes NEO-ddCOSMO derivation, solvation free energies for the water dimer with all possible NEO partitions, and difference in electrostatic solvation free energy per proton between NEO and conventional calculations using C-PCM and SS(V)PE.

Acknowledgements

The development of solvated NEO methods in the Chronus Quantum computational software is supported by the Department of Energy in the Computational Chemical Science program (Grant No. DE-SC0023284). The software infrastructure, including NEO integrals and self-consistent-field, is supported by the Office of Advanced Cyberinfrastructure, National Science Foundation (Grant No. OAC-2103717 and OAC-2103902). The study of reactions in aqueous environments is supported by IDREAM (Interfacial Dynamics in Radioactive Environments and Materials), an Energy Frontier Research Center funded by the U.S. Department of Energy (DOE), Office of Science, Basic Energy Sciences (FWP 68932). All figures in this

paper were generated using Matplotlib.[66] Molecular graphics were visualized using UCSF Chimera.[67]

References

(1) Mennucci, B. Polarizable Continuum Model. *WIREs Comput. Mol. Sci.* **2012**, *2*, 386–404.

(2) Herbert, J. M. Dielectric Continuum Methods for Quantum Chemistry. *WIREs Comput. Mol. Sci.* **2021**, *11*, e1519.

(3) Klamt, A.; Schüürmann, G. COSMO: A New Approach to Dielectric Screening in Solvents With Explicit Expressions for the Screening Energy and Its Gradient. *J. Chem. Soc. Perkin Trans.* **1993**, 799–805.

(4) Barone, V.; Cossi, M. Quantum Calculation of Molecular Energies and Energy Gradients in Solution by a Conductor Solvent Model. *J. Phys. Chem. A* **1998**, *102*, 1995–2001.

(5) Cossi, M.; Rega, N.; Scalmani, G.; Barone, V. Energies Structures and Electronic Properties of Molecules in Solution With the C-PCM Solvation Model. *J. Comput. Chem.* **2003**, *24*, 669–681.

(6) Klamt, A.; Moya, C.; Palomar, J. A Comprehensive Comparison of the IEFPCM and SS (V) PE Continuum Solvation Methods With the COSMO Approach. *J. Chem. Theory Comput.* **2015**, *11*, 4220–4225.

(7) Lipparini, F.; Mennucci, B. Hybrid QM/classical models: Methodological advances and new applications. *Chem. Phys. Rev.* **2021**, *2*, 041303.

(8) Webb, S. P.; Iordanov, T.; Hammes-Schiffer, S. Multiconfigurational Nuclear-Electronic

Orbital Approach: Incorporation of Nuclear Quantum Effects in Electronic Structure Calculations. *J. Chem. Phys.* **2002**, *117*, 4106–4118.

(9) Althorpe, S. C. Path-Integral Approximations to Quantum Dynamics. *Euro. Phys. J. B* **2021**, *94*, 155.

(10) Habershon, S.; Manolopoulos, D. E.; Markland, T. E.; Miller III, T. F. Ring-Polymer Molecular Dynamics: Quantum Effects in Chemical Dynamics From Classical Trajectories in an Extended Phase Space. *Annu. Rev. Phys. Chem.* **2013**, *64*, 387–413.

(11) Zhao, L.; Tao, Z.; Pavošević, F.; Wildman, A.; Hammes-Schiffer, S.; Li, X. Real-Time Time-Dependent Nuclear-Electronic Orbital Approach: Dynamics Beyond the Born-Oppenheimer Approximation. *J. Phys. Chem. Lett.* **2020**, *11*, 4052–4058.

(12) Zhao, L.; Wildman, A.; Tao, Z.; Schneider, P.; Hammes-Schiffer, S.; Li, X. Nuclear–Electronic Orbital Ehrenfest Dynamics. *J. Chem. Phys.* **2020**, *153*, 224111.

(13) Zhao, L.; Wildman, A.; Pavošević, F.; Tully, J. C.; Hammes-Schiffer, S.; Li, X. Excited State Intramolecular Proton Transfer with Nuclear-Electronic Orbital Ehrenfest Dynamics. *J. Phys. Chem. Lett.* **2021**, *12*, 3497–3502.

(14) Tao, Z.; Yu, Q.; Roy, S.; Hammes-Schiffer, S. Direct Dynamics With Nuclear–Electronic Orbital Density Functional Theory. *Acc. Chem. Res.* **2021**, *54*, 4131–4141.

(15) Wildman, A.; Tao, Z.; Zhao, L.; Hammes-Schiffer, S.; Li, X. Solvated Nuclear–Electronic Orbital Structure and Dynamics. *J. Chem. Theory Comput.* **2022**, *18*, 1340–1346.

(16) Pak, M. V.; Chakraborty, A.; Hammes-Schiffer, S. Density Functional Theory Treatment of Electron Correlation in the Nuclear- Electronic Orbital Approach. *J. Phys. Chem. A* **2007**, *111*, 4522–4526.

(17) Yang, Y.; Brorsen, K. R.; Culpitt, T.; Pak, M. V.; Hammes-Schiffer, S. Development of a Practical Multicomponent Density Functional for Electron-Proton Correlation to Produce Accurate Proton Densities. *J. Chem. Phys.* **2017**, *147*, 114113.

(18) Brorsen, K. R.; Yang, Y.; Hammes-Schiffer, S. Multicomponent Density Functional Theory: Impact of Nuclear Quantum Effects on Proton Affinities and Geometries. *J. Phys. Chem. Lett.* **2017**, *8*, 3488–3493.

(19) Swalina, C.; Pak, M. V.; Hammes-Schiffer, S. Alternative Formulation of Many-Body Perturbation Theory for Electron–Proton Correlation. *Chem. Phys. Rev.* **2005**, *404*, 394–399.

(20) Pavošević, F.; Culpitt, T.; Hammes-Schiffer, S. Multicomponent Coupled Cluster Singles and Doubles Theory Within the Nuclear-Electronic Orbital Framework. *J. Chem. Theory Comput.* **2018**, *15*, 338–347.

(21) Pavošević, F.; Culpitt, T.; Hammes-Schiffer, S. Multicomponent Quantum Chemistry: Integrating Electronic and Nuclear Quantum Effects via the Nuclear–Electronic Orbital Method. *Chem. Rev.* **2020**, *120*, 4222–4253.

(22) Foresman, J. B.; Keith, T. A.; Wiberg, K. B.; Snoonian, J.; Frisch, M. J. Solvent Effects. 5. Influence of Cavity Shape Truncation of Electrostatics and Electron Correlation on Ab Initio Reaction Field Calculations. *J. Phys. Chem.* **1996**, *100*, 16098–16104.

(23) Barone, V.; Cossi, M.; Tomasi, J. A New Definition of Cavities for the Computation of Solvation Free Energies by the Polarizable Continuum Model. *J. Chem. Phys.* **1997**, *107*, 3210–3221.

(24) Klamt, A.; Jonas, V. Treatment of the Outlying Charge in Continuum Solvation Models. *J. Chem. Phys.* **1996**, *105*, 9972–9981.

(25) Chipman, D. M. Reaction Field Treatment of Charge Penetration. *J. Chem. Phys.* **2000**, *112*, 5558–5565.

(26) Cancès, E.; Mennucci, B. Comment on "Reaction Field Treatment of Charge Penetration". *J. Chem. Phys.* **2001**, *114*, 4744–4745.

(27) Miertuš, S.; Scrocco, E.; Tomasi, J. Electrostatic Interaction of a Solute With a Continuum. A Direct Utilizaion of AB Initio Molecular Potentials for the Prevision of Solvent Effects. *Chem. Phys.* **1981**, *55*, 117–129.

(28) Lipparini, F.; Scalmani, G.; Mennucci, B.; Cancès, E.; Caricato, M.; Frisch, M. J. a Variational Formulation of the Polarizable Continuum Model. *J. Chem. Phys.* **2010**, *133*, 014106.

(29) Chipman, D. M. Simulation of Volume Polarization in Reaction Field Theory. *J. Chem. Phys.* **1999**, *110*, 8012–8018.

(30) Chipman, D. M. New Formulation and Implementation for Volume Polarization in Dielectric Continuum Theory. *J. Chem. Phys.* **2006**, *124*, 224111.

(31) Cances, E.; Mennucci, B.; Tomasi, J. a New Integral Equation Formalism for the Polarizable Continuum Model: Theoretical Background and Applications to Isotropic and Anisotropic Dielectrics. *J. Chem. Phys.* **1997**, *107*, 3032–3041.

(32) Mennucci, B.; Cances, E.; Tomasi, J. Evaluation of Solvent Effects in Isotropic and Anisotropic Dielectrics and in Ionic Solutions With a Unified Integral Equation Method: Theoretical Bases Computational Implementation and Numerical Applications. *J. Phys. Chem. B* **1997**, *101*, 10506–10517.

(33) Cancès, E.; Mennucci, B. New Applications of Integral Equations Methods for Solvation Continuum Models: Ionic Solutions and Liquid Crystals. *J. Math. Chem.* **1998**, *23*, 309–326.

(34) Stefanovich, E. V.; Truong, T. N. Optimized Atomic Radii for Quantum Dielectric Continuum Solvation Models. *Chem. Phys. Rev.* **1995**, *244*, 65–74.

(35) Truong, T. N.; Stefanovich, E. V. A New Method for Incorporating Solvent Effect Into the Classical Ab Initio Molecular Orbital and Density Functional Theory Frameworks for Arbitrary Shape Cavity. *Chem. Phys. Rev.* **1995**, *240*, 253–260.

(36) Truong, T. N.; Stefanovich, E. V. Hydration Effects on Reaction Profiles: An Ab Initio Dielectric Continuum Study of the SN2 Cl-+ CH3Cl Reaction. *J. Phys. Chem.* **1995**, *99*, 14700–14706.

(37) Truong, T. N.; Stefanovich, E. V. Analytical First and Second Energy Derivatives of the Generalized Conductorlike Screening Model for Free Energy of Solvation. *J. Chem. Phys.* **1995**, *103*, 3709–3717.

(38) Truong, T. N.; Nguyen, U. N.; Stefanovich, E. V. Generalized Conductor-Like Screening Model (GCOSMO) for Solvation: An Assessment of Its Accuracy and Applicability. *Int. J. Quant. Chem.* **1996**, *60*, 1615–1622.

(39) Lambros, E.; Link, B.; Chow, M.; Hammes-Schiffer, S.; Li, X. Solvent Induced Proton Polarization within the Nuclear–Electronic Orbital Framework. *J. Phys. Chem. Lett.* **2023**, *14*, 2990–2995.

(40) Chow, M.; Lambros, E.; Li, X.; Hammes-Schiffer, S. Nuclear–Electronic Orbital QM/MM Approach: Geometry Optimizations and Molecular Dynamics. *J. Chem. Theory Comput.* **2023**, *19*, 3839–3848.

(41) Kanematsu, Y.; Tachikawa, M. Development of Multicomponent Hybrid Density Functional Theory With Polarizable Continuum Model for the Analysis of Nuclear Quantum Effect and Solvent Effect on NMR Chemical Shift. *J. Chem. Phys.* **2014**, *140*, 164111.

(42) Kanematsu, Y.; Tachikawa, M. Performance Test of Multicomponent Quantum Mechanical Calculation With Polarizable Continuum Model for Proton Chemical Shift. *J. Phys. Chem. A* **2015**, *119*, 4933–4938.

(43) Babin, V.; Leforestier, C.; Paesani, F. Development of a "First Principles" Water Potential With Flexible Monomers: Dimer Potential Energy Surface VRT Spectrum and Second Virial Coefficient. *J. Chem. Theory Comput.* **2013**, *9*, 5395–5403.

(44) Babin, V.; Medders, G. R.; Paesani, F. Development of a "First Principles" Water Potential With Flexible Monomers. II: Trimer Potential Energy Surface Third Virial Coefficient and Small Clusters. *J. Chem. Theory Comput.* **2014**, *10*, 1599–1607.

(45) Medders, G. R.; Babin, V.; Paesani, F. Development of a "First Principles" Water Potential With Flexible Monomers. III. Liquid Phase Properties. *J. Chem. Theory Comput.* **2014**, *10*, 2906–2910.

(46) Chakraborty, A.; Pak, M. V.; Hammes-Schiffer, S. Properties of the Exact Universal Functional in Multicomponent Density Functional Theory. *J. Chem. Phys.* **2009**, *131*, 124115.

(47) Lipparini, F.; Stamm, B.; Cances, E.; Maday, Y.; Mennucci, B. Fast Domain Decomposition Algorithm for Continuum Solvation Models: Energy and First Derivatives. *J. Chem. Theory Comput.* **2013**, *9*, 3637–3648.

(48) Lipparini, F.; Scalmani, G.; Lagardère, L.; Stamm, B.; Cancès, E.; Maday, Y.; Piquemal, J.-P.; Frisch, M. J.; Mennucci, B. Quantum Classical and Hybrid QM/MM Calculations in Solution: General Implementation of the ddCOSMO Linear Scaling Strategy. *J. Chem. Phys.* **2014**, *141*, 184108.

(49) Stamm, B.; Lagardère, L.; Scalmani, G.; Gatto, P.; Cancès, E.; Piquemal, J.-P.; Maday, Y.; Mennucci, B.; Lipparini, F. How to Make Continuum Solvation Incredibly Fast

in a Few Simple Steps: A Practical Guide to the Domain Decomposition Paradigm for the Conductor-Like Screening Model. *Int. J. Quant. Chem.* **2019**, *119*, e25669.

(50) Stamm, B.; Cancès, E.; Lipparini, F.; Maday, Y. A New Discretization for the Polarizable Continuum Model Within the Domain Decomposition Paradigm. *J. Chem. Phys.* **2016**, *144*, 054101.

(51) Mikhalev, A.; Nottoli, M.; Stamm, B. Linearly Scaling Computation of ddPCM Solvation Energy and Forces Using the Fast Multipole Method. *J. Chem. Phys.* **2022**, *157*, 114103.

(52) Reddy, S. K.; Straight, S. C.; Bajaj, P.; Huy Pham, C.; Riera, M.; Moberg, D. R.; Morales, M. A.; Knight, C.; Götz, A. W.; Paesani, F. on the Accuracy of the MB-pol Many-Body Potential for Water: Interaction Energies Vibrational Frequencies and Classical Thermodynamic and Dynamical Properties From Clusters to Liquid Water and Ice. *J. Chem. Phys.* **2016**, *145*, 194504.

(53) Lambros, E.; Paesani, F. How good are polarizable and flexible models for water: Insights from a many-body perspective. *The Journal of Chemical Physics* **2020**, *153*, 060901.

(54) Lambros, E.; Lipparini, F.; Cisneros, G. A.; Paesani, F. A many-body, fully polarizable approach to QM/MM simulations. *Journal of chemical theory and computation* **2020**, *16*, 7462–7472.

(55) Williams-Young, D. B.; Petrone, A.; Sun, S.; Stetina, T. F.; Lestrange, P.; Hoyer, C. E.; Nascimento, D. R.; Koulias, L.; Wildman, A.; Kasper, J.; Goings, J. J.; Ding, F.; DePrince III, A. E.; Valeev, E. F.; Li, X. The Chronus Quantum (ChronusQ) Software Package. *WIREs Comput. Mol. Sci.* **2020**, *10*, e1436.

(56) Adamo, C.; Barone, V. Toward Reliable Density Functional Methods Without Adjustable Parameters: The PBE0 Model. *J. Chem. Phys.* **1999**, *110*, 6158–6170.

(57) Rezac, J.; Hobza, P. Describing Noncovalent Interactions Beyond the Common Approximations: How Accurate Is the "Gold Standard" CCSD (T) at the Complete Basis Set Limit? *J. Chem. Theory Comput.* **2013**, *9*, 2151–2155.

(58) Epifanovsky, E.; Gilbert, A. T.; Feng, X.; Lee, J.; Mao, Y.; Mardirossian, N.; Pokhilko, P.; White, A. F.; Coons, M. P.; Dempwolff, A. L., et al. Software for the Frontiers of Quantum Chemistry: An Overview of Developments in the Q-Chem 5 Package. *J. Chem. Phys.* **2021**, *155*, 084801.

(59) Sun, Q.; Berkelbach, T. C.; Blunt, N. S.; Booth, G. H.; Guo, S.; Li, Z.; Liu, J.; McClain, J. D.; Sayfutyarova, E. R.; Sharma, S., et al. PySCF: The Python-Based Simulations of Chemistry Framework. *WIREs Comput. Mol. Sci.* **2018**, *8*, e1340.

(60) Sun, Q.; Zhang, X.; Banerjee, S.; Bao, P.; Barbry, M.; Blunt, N. S.; Bogdanov, N. A.; Booth, G. H.; Chen, J.; Cui, Z.-H., et al. Recent Developments in the PySCF Program Package. *J. Chem. Phys.* **2020**, *153*, 024109.

(61) Dunning Jr, T. H. Gaussian Basis Sets for Use in Correlated Molecular Calculations. I. The Atoms Boron Through Neon and Hydrogen. *J. Chem. Phys.* **1989**, *90*, 1007–1023.

(62) Yu, Q.; Pavošević, F.; Hammes-Schiffer, S. Development of Nuclear Basis Sets for Multicomponent Quantum Chemistry Methods. *J. Chem. Phys.* **2020**, *152*, 244123.

(63) Riera, M.; Knight, C.; Bull-Vulpe, E. F.; Zhu, X.; Smith, D. G.; Simmonett, A. C.; Paesani, F. MBX: A many-body energy and force calculator for data-driven many-body simulations. *ChemRxiv* **2023**,

(64) Liu, A.; Chow, M.; Wildman, A.; Frisch, M. J.; Hammes-Schiffer, S.; Li, X. Simultaneous Optimization of Nuclear–Electronic Orbitals. *J. Phys. Chem. A* **2022**, *126*, 7033–7039.

(65) Reddy, S. K.; Moberg, D. R.; Straight, S. C.; Paesani, F. Temperature-dependent vibrational spectra and structure of liquid water from classical and quantum simulations with the MB-pol potential energy function. *The Journal of Chemical Physics* **2017**, *147*, 244504.

(66) Hunter, J. D. Matplotlib: A 2D Graphics Environment. *Comput. Sci. Eng.* **2007**, *9*, 90–95.

(67) Pettersen, E. F.; Goddard, T. D.; Huang, C. C.; Couch, G. S.; Greenblatt, D. M.; Meng, E. C.; Ferrin, T. E. UCSF Chimera—A Visualization System for Exploratory Research and Analysis. *J. Comput. Chem.* **2004**, *25*, 1605–1612.

TOC Graphic

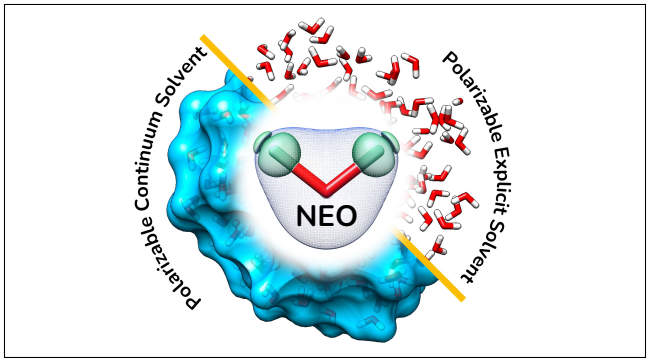
Polarizable Continuum Solvent
Polarizable Explicit Solvent
NEO